Experimental observation of electron-phonon coupling enhancement in Sn nanowires caused by phonon confinement effects

D. P. Lozano,[1] S. Couet,[1] C. Petermann,[1] G. Hamoir,[2] J. K. Jochum,[3] T. Picot,[3] E. Menéndez,[1,4] K. Houben,[3] V. Joly,[1] V. A. Antohe,[2,5] Michael Y. Hu,[6] B. M. Leu,[6,7] A. Alatas,[6] Ayman H. Said,[6] S. Roelants,[8] B. Partoens,[8] M. V. Milošević,[8] F. M. Peeters,[8] L. Piraux,[2] J. Van de Vondel,[3] A. Vantomme,[1] K. Temst,[1] and M. J. Van Bael[3]

[1]*KU Leuven, Instituut voor Kern-en Stralingsfysica, Celestijnenlaan 200 D, 3001 Leuven, Belgium*

[2]*Institute of Condensed Matter and Nanosciences (IMCN), Université catholique de Louvain, Place Croix du Sud 1, 1348 Louvain-la-Neuve, Belgium*

[3]*Laboratory of Solid-State Physics and Magnetism, KU Leuven, Celestijnenlaan 200D, 3001 Leuven, Belgium*

[4]*Departament de Física, Universitat Autònoma de Barcelona, E-08193 Cerdanyola del Vallès, Spain*

[5]*Research and Development Center for Materials and Electronic & Optoelectronic Devices (MDEO), Faculty of Physics, University of Bucharest, Atomistilor str. 405, 077125 Bucharest-Magurele, Romania*

[6]*Advanced Photon Source, Argonne National Laboratory, Argonne, Illinois 60439, USA*

[7]*Department of Physics, Miami University, Oxford, Ohio 45056, USA*

[8]*Departement Fysica, Universiteit Antwerpen, Groenenborgerlaan 171, B-2020 Antwerpen, Belgium*

(Received 31 January 2018; revised manuscript received 11 January 2019; published 21 February 2019)

Reducing the size of a superconductor below its characteristic length scales can either enhance or suppress its critical temperature (T_c). Depending on the bulk value of the electron-phonon coupling strength, electronic and phonon confinement effects will play different roles in the modification of T_c. Experimentally disentangling each contribution has remained a challenge. We have measured both the phonon density of states and T_c of Sn nanowires with diameters of 18, 35, and 100 nm in order to quantify the effects of phonon confinement on superconductivity. We observe a shift of the phonon frequency towards the low-energy region and an increase in the electron-phonon coupling constant that can account for the measured increase in T_c.

DOI: 10.1103/PhysRevB.99.064512

I. INTRODUCTION

The electron-phonon interaction plays a fundamental role in electrical transport [1], thermal conductivity [2], and many-body phenomena such as superconductivity [3]. In reduced dimensions, the strength of this interaction is modified due to size effects in both, electronic levels and phonon spectrum. For instance, nanostructuring superconductors leads to dramatic changes in their properties compared to their bulk counterparts. These changes appear mostly once the size of the superconductor becomes smaller than the coherence length ξ_0 resulting in a modification of the critical temperature T_c [4], the critical magnetic field H_c [5,6], and the superconducting gap Δ_0 [7]. Particularly, the behavior of T_c has received a lot of interest since its modification depends on how nanostructuring affects the electron-phonon interaction (e-ph), reflected in the value of the electron-phonon coupling constant $\lambda_{\text{e-ph}}$ [8].

Nanostructured weak-coupling superconductors show a progressive enhancement of T_c with a decrease of the characteristic dimension of the system. An increase of T_c of about 25% with respect to bulk Al has been observed in Al nanowires with 8 nm diameter [9], while in Sn nanowires with 20 nm diameter, the enhancement was only about 10% [10]. For In nanoparticles with 36 nm diameter, the T_c increase was smaller, only about 5% [11]. This T_c enhancement has generally been attributed to an enhancement of the electron-phonon coupling caused by surface phonon modes and crystallite boundaries [12]. On the other hand, T_c of strong-coupling materials seems not to be severely affected by dimensional effects. The T_c of Pb nanoparticles decreases slightly within a diameter range spanning from 65 nm down to 7 nm [13], after which T_c drops abruptly. In the case of Nb, a progressive decrease of T_c was observed in nanowires with diameter between 420 and 80 nm [14]. However, these materials are equally affected by surface and boundary effects as weak-coupling superconductors are, since those are a consequence of the sample's geometry. This has been demonstrated in Pb nanoparticles embedded into nanoporous glass [15]. Therefore a mechanism that opposes the enhancement of $\lambda_{\text{e-ph}}$ should be present.

There exist two effects that play an important role in the T_c modification of nanoscale superconductors. First, oscillations of the mean electron density near the Fermi level as a consequence of the discretization of the energy levels in reduced dimensions, known as quantum size effects (QSE) [16], and second, the shift of phonon modes towards low energies as a consequence of phonon confinement, known as phonon softening [17]. Phonon softening is expected to increase T_c, while the influence of QSE depends on the electron-phonon coupling strength. Even a combination of these two effects can explain the observed T_c behavior. Phonon softening has been observed in Sn and Pb nanoparticles embedded into porous glass [15,18]. However, no link with the effect on T_c was established. Similar measurements were carried out in Nb_3Sn thin films [19], where the role of phonon softening was quantified, revealing that its contribution was not enough to explain the change of T_c. QSE were pointed out as the main effect responsible for this change.

Disentangling and quantifying the individual effects of phonon softening and QSE remains a challenge, mainly due to the lack of techniques capable of measuring phonons in nanoscale superconductors. Electron tunneling experiments in superconducting junctions [20] are able to provide information about the electron-phonon interaction; however, they are intrinsically influenced by electronic effects. Therefore techniques that allow for the differentiation between these two effects are required.

In this work, we quantify the contribution of phonon softening effects to the modification of T_c in nanoscale superconductors. Measuring the phonon density of states $F(E)$ of Sn nanowire arrays embedded in porous alumina (Al_2O_3) matrices with different pore diameters using nuclear resonant inelastic x-ray scattering (NRIXS) allows us to determine the shifting of the phonon frequencies and the increment of the electron-phonon coupling upon decreasing diameter. The combination of these results with data from transport measurements suggests that phonon softening is responsible for the T_c enhancement observed in the Sn nanowire samples studied.

II. SAMPLE PREPARATION AND STRUCTURAL CHARACTERIZATION

Tin nanowire arrays were synthesized by electrodepositing Sn from an aqueous electrolyte containing 7 g/L $C_4H_6O_6$, 115 g/L $Na_4P_2O_7 \cdot 10H_2O$, 30 g/L $^{119}SnCl_2 \cdot 2H_2O$, and 0.4 g/L gelatin [21] into 50-μm-thick nanoporous Al_2O_3 membranes with pore diameters of 18 ± 3, 35 ± 3, and 100 ± 10 nm. A bilayer consisting of 10 nm of Cr followed by 300 nm of Au was deposited by e-beam evaporation on one side of the membranes to serve as working electrode. Isotopically enriched $^{119}SnCl_2 \cdot 2H_2O$ was developed in house due to the lack of its commercial availability. The electrochemical growth of homogenous nanowires within the Al_2O_3 membranes was carried out in a three-electrode potentiostatic configuration by applying to the working electrode -0.9 V versus a double-junction Ag/AgCl reference electrode (KCl saturated, $E = 0.197$ V), while a Pt foil was installed in the bath as a counter electrode. The process was stopped once the Sn overfilled the membrane. In order to check the reproducibility of the critical temperature, two samples with diameters of 35 nm (samples c and d) and two samples with diameters of 100 nm (samples g and h) were prepared using this method. Due to proximity effects the top and/or bottom layer can significantly affect the T_c of the nanowires [22]. To identify the importance of this effect, nanowires overgrown with Cu were fabricated as well. For these samples, the growth within the membranes was stopped once the wires reached 25 μm and then Cu was electrodeposited to fill the rest of the template. Samples with diameters of 35 nm (samples e and f) and 18 nm (samples a and b) were prepared using this method. After the growth process the membranes where taken out of the electrolyte in order to characterize the samples. Additionally, three more samples with nanowire diameters of 18, 35, and 100 nm were grown using the Mössbauer isotope ^{119}Sn in order to perform the NRIXS measurements. The latter set of samples was not overgrown in order to avoid the contribution of unconfined nanowire caps on the template surface to the NRIXS measurements. As shown in the cross-sectional scanning electron microscope (SEM) image in Fig. 1(a), the samples are formed by an array of vertically aligned nanowires. The diameter of the nanowires slightly fluctuates along the longitudinal direction, its standard deviations are 6, 2, and 1.5 nm for the 100, 35, and 18 nm samples.

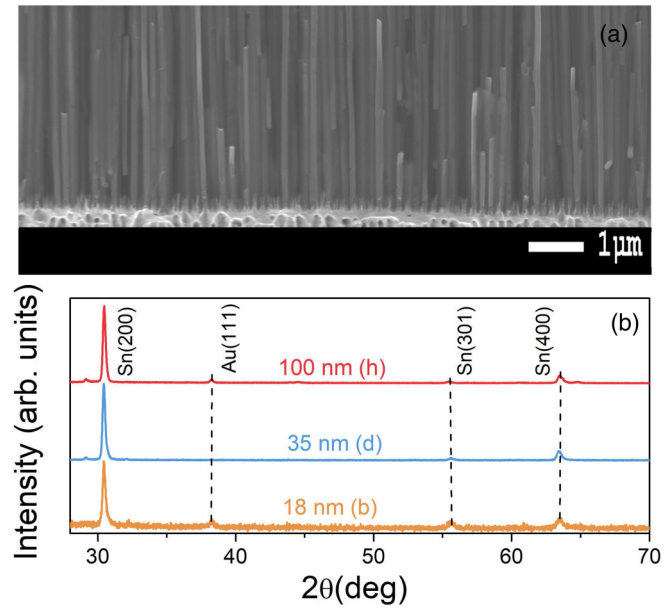

FIG. 1. (a) SEM image of a 50 μm membrane containing Sn nanowires with a diameter of 100 nm. (b) XRD spectra for the Sn nanowires embedded in Al_2O_3 porous matrices with different pore diameter.

Structural characterization was performed by $\theta/2\theta$ x-ray diffraction (XRD) and grazing incidence XRD (GIXRD) with an incidence angle of 4°, using Cu $K_{\alpha 1}$ radiation. Figure 1(b) shows the XRD patterns for the three types of samples investigated. In all samples, three peaks corresponding to β-Sn can be observed at approximately 30°, 56°, and 63°. In addition, an Au peak arises from the cathode at 38°. The $\theta/2\theta$ XRD patterns of all samples are consistent with a polycrystalline array of nanowires containing a highly textured β-Sn phase oriented along (200) planes with traces of (301) oriented planes. GIXRD measurements (available in Ref. [23]) show either no peaks or tiny traces of the (200) β-Sn peak just above the background level, confirming the strong texture of the β-Sn nanowires. To obtain the (average coherently diffracting) crystallite size of the β-Sn phase along the direction of the wires, Rietveld refinement [24] of the $\theta/2\theta$ XRD patterns was performed using the MAUD software [25]. The grain size of the 35-nm- and 100-nm-diameter samples is larger than 200 nm and cannot be resolved by line profile analysis [26], while a grain size of 185 nm is found for the 18-nm-diameter sample, indicating that the nanowires consist of a series of strongly elongated grains along their axis.

III. SUPERCONDUCTING PROPERTIES

Transport measurements were performed by making four contacts on the sample, two on the top surface and two at the bottom. A schematic drawing of the contact geometry

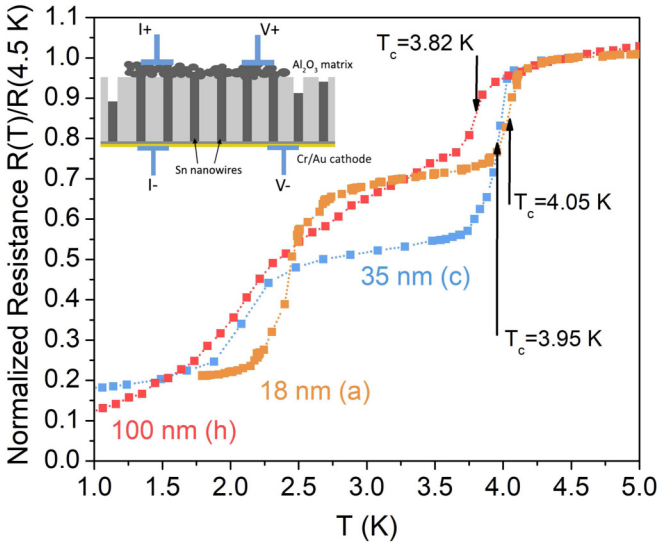

FIG. 2. Normalized resistance measurement of the Sn nanowires. The diameters of the nanowires are 100 (h, red), 35 (c, blue), and 18 nm (a, orange). The black arrows indicate the critical temperature defined according to the criterion explained in the text. The inset depicts a sketch of the measurement configuration.

is shown in the inset of Fig. 2. The normalized resistance $R(T)/R(4.5\ \mathrm{K})$ of three representative samples (one of each thickness) as a function of temperature are displayed in Fig. 2, showing a distinct number of features. Marked with black arrows, a first resistance drop occurs around 4 K. Beyond this transition and towards lower temperatures, the resistance does not drop to zero, but it slowly decreases until a second transition is visible in a temperature rage around 2.25 K. After this transition, the zero resistance state is still not reached. The normalized resistance curves of the other samples can be found in the supplementary information. In general, for each nanowire diameter the obtained transitions display a very similar behavior.

We attribute the first resistance drop to the superconducting transition of the strongly elongated grains forming the nanowires. In this viewpoint, T_c is defined as the middle point of this transition, thus obtaining values of 4.05 ± 0.05, 3.95 ± 0.05, and 3.82 ± 0.05 K for the 18, 35, and 100 nm, respectively. Moreover, the comparison between Sn overgrown and Cu overgrown samples directly shows that the overgrown layer does not impact the obtained T_c. This represents an enhancement of up to 10% compared to 3.72 K, the bulk T_c value. These values of T_c are in agreement with the values observed in other Sn nanowire systems [10,27,28]. The second resistance drop occurs in a temperature range between 2.0 and 2.5 K. While the first superconducting transition is related to the local superconductivity within the narrow elongated grains of the individual nanowires; we hypothesize that the second transition is related to the emergence of long-range superconductivity when coupling between these grains is established at lower temperatures. This feature will be the topic of future work.

In addition to the two resistance drops observed, a third one would be expected around 3.7 K in the Sn overgrown samples due to the superconducting transition of the bulk overgrown layer. However, such a transition only appears in the magnetoresistance curve of one of the Sn overgrown 35-nm samples (sample c), shown in Ref. [23], and not in the resistance versus temperature curve in Fig. 2. Figure S3 in Ref. [23] shows a narrow transition appearing already at 3.7 K and visible in the entire temperature range explored. It can be suppressed by applying a magnetic field of about 0.05 T at 1 K. This value is comparable to the critical magnetic field of bulk Sn [29], therefore, this transition is likely caused by the bulk Sn layer. The 100-nm and one of the 35-nm Sn overgrown samples (samples g, h, and d) present only two transitions. One possible explanation for the absence of the superconducting transition in the overgrown layer could be that the large contact area of this layer contributed to a very small fraction of the system's total resistance. Then, the decrease in resistance caused by the superconducting transition of the overgrown layer would be too small to be discernible in our data. The noise level in the 100 nm samples is 1 mV, while it is 0.5 mV in the 35 nm sample (sample d). On the other hand, the resistance drop caused by the overgrown layer in the 35 nm sample (sample c) is only 0.15 mV. Therefore the effect of the overgrown layer's superconducting transition is hidden by the noise in samples g, h, and d. Tian *et al.* studied Sn nanowires with diameter ranging from 20 to 160 nm embedded in porous matrices contacted by bulk Sn electrodes [10,30]. Similar to our resistance versus temperature data, their data do not show any evidence of the superconducting transition in the bulk Sn electrodes.

The superconducting phase boundaries can provide additional evidence to our interpretation of the first resistance drop, since strong dimensional effects are expected in their temperature dependence due to the confined geometry of the grains forming the nanowires. The superconducting phase boundaries were determined measuring the magnetoresistance of the nanowires at different temperatures while an external magnetic field was applied perpendicular to the nanowires axis (see Ref. [23]). The magnetic field corresponding to 90% of the resistance between the normal and the lowest resistance state was used as criterion for H_c. This criterion is used to guarantee that the phase boundaries are determined using values of the resistance similar to those used for determining the T_c of the first transition. Results are shown in Fig. 3. The superconducting region significantly increases as the diameter is reduced. The solid lines are fittings to the experimental data using Eq. (1) [31]

$$H_c(T) = \frac{\sqrt{3}\phi_0}{\pi d \mu_0 \xi_{\mathrm{GL}}(0)} \sqrt{1 - \frac{T}{T_c}}, \tag{1}$$

where ϕ_0 is the magnetic flux quantum, d is the diameter of the nanowires, and $\xi_{\mathrm{GL}}(0)$ is the Ginzburg-Landau coherence length at 0 K. This last one was used as a fitting parameter. There is a good correspondence between Eq. (1) and the experimental data, especially at temperatures close to T_c. Note that this relationship between $H_c(T)$ and T is typically observed in narrow superconducting lines [32], rather than the characteristic linear relationship observed in bulk superconductors [33], as we had anticipated, and confirms that the first resistance drop and consequently T_c corresponds to the nanowires. This, together with the strong diameter

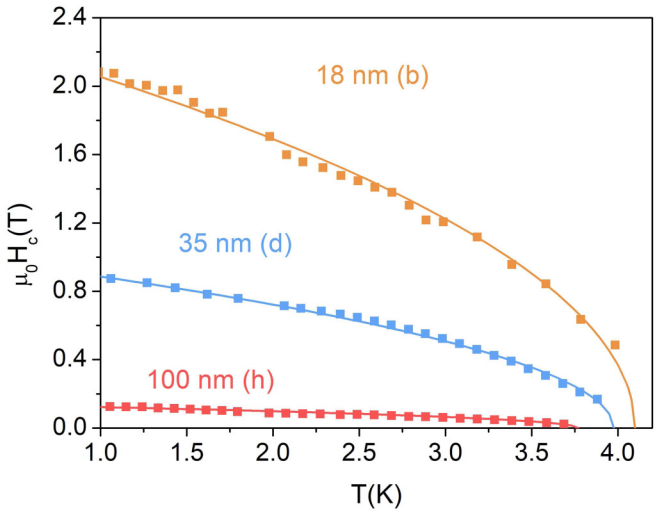

FIG. 3. Superconducting phase boundaries for the 18 nm (b, orange), 35 nm (d, blue), and 100 nm (h, red) samples, when a magnetic field is applied perpendicular to the nanowires axis.

dependence of the critical field confirms that the critical field probed corresponds to the nanowires.

The $\xi_{GL}(0)$ values obtained from the phase boundary fittings are shown in Fig. 4. Note that Eq. (1) strictly applies to a narrow superconducting line of rectangular cross-section and thickness d in a perpendicular magnetic field [32]. The $\xi_{GL}(0)$ values should be considered an estimation to the coherence length, where the diameter of the wire plays the role of the line thickness. $\xi_{GL}(0)$ is significantly smaller than $\xi_{GL}(0)$ for bulk Sn [10], and it decreases monotonically as the nanowire diameter is reduced. This suggests that our nanowires are in the dirty limit since $\xi_{GL}(0)$ is expected to decrease in nanostructured dirty superconductors [34] with decreasing particle size as a consequence of the reduction in the effective mean free path [35].

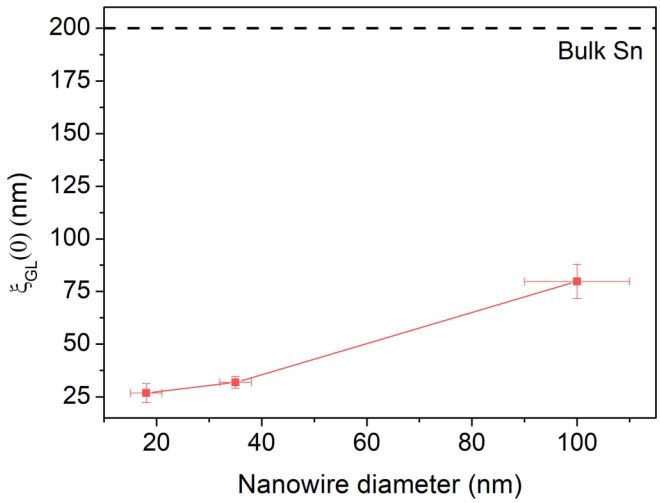

FIG. 4. Coherence length (red squares) of the 18 nm, 35 nm, and 100 nm samples when a magnetic field is applied perpendicular to their longitudinal axis compared to the bulk value (black dashed line). The red line is a guide to the eye.

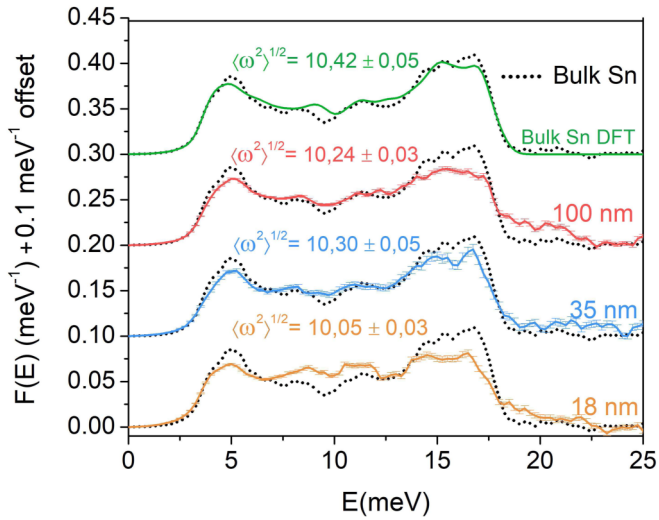

FIG. 5. Phonon density of states of bulk Sn calculated using DFT methods (green) and of membranes containing nanowires of 100 nm, 35 nm, and 18 nm diameter (red, blue, and orange, respectively) taken at 20 K. The black dotted curve represents the $F(E)$ of a bulk Sn foil measured during a previous experiment [42].

IV. PHONON DENSITY OF STATES

The phonon density of states of the nanowires was measured using NRIXS [36]. This technique allows the extraction of $F(E)$ corresponding to only the Mössbauer-active material, ^{119}Sn in this case. No contributions from other atoms are measured, unlike inelastic neutron scattering (INS) or inelastic x-ray scattering (IXS). Moreover, the determination of F(E) from the NRIXS is model independent and it has been successfully applied to other nanosystems [37]. Measurements were performed at sector 30 of the Advanced Photon Source (APS). Details of the experimental set up are reported elsewhere [38]. The measured spectra consist of the photon count rate as a function of the energy difference between the incident photon and the Mössbauer nuclear transition in ^{119}Sn. The set of samples used in the measurement are 99% isotopically enriched ^{119}Sn nanowires, not overgrown. Therefore the recorded spectra correspond uniquely to the nanowires. The NRIXS scans were taken in two different configurations: the x-ray beam parallel and perpendicular to the nanowires axis. The spectra were converted to $F(E)$ following the procedure described by Sturhahn [39] and using the PHOENIX software [40]. For each configuration, the partial $F(E)$ was derived (see Ref. [23]) and summed according to the following ratio: $\frac{2}{3}F(E)_{\text{perpendicular}} + \frac{1}{3}F(E)_{\text{parallel}}$ [41], in order to obtain the complete $F(E)$ of the sample.

Figure 5 shows the $F(E)$'s obtained for the different samples together with the bulk Sn $F(E)$ calculated using density functional theory (DFT) and convoluted with the experimental resolution function. All of them are compared to the $F(E)$ of a Sn foil. The calculated $F(E)$ is in good agreement with the Sn foil $F(E)$, especially in the low and high energy parts; even the Sn cut off energy is accurately predicted. A number of significant differences are observed when comparing the phonon spectra of the nanowires and bulk Sn. The intensity of the high-energy phonon modes at 15 and

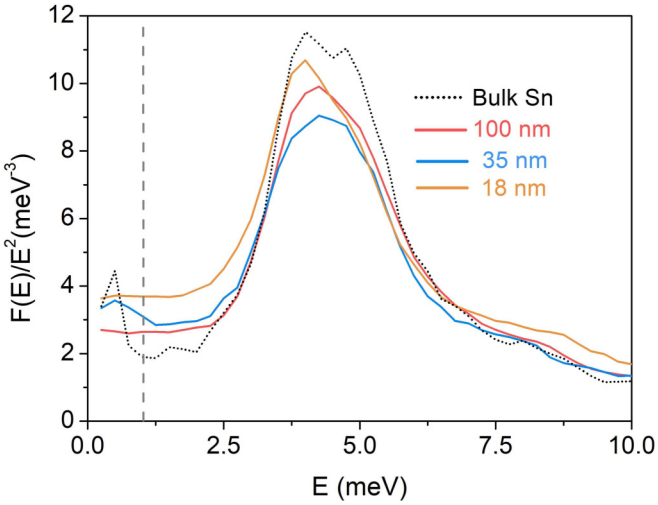

FIG. 6. Reduced phonon density of states $[F(E)/E^2]$ over an energy region from 0 to 10 meV, of Sn nanowires with diameters of 100 nm, 35 nm, and 18 nm diameter (red, blue, and orange, respectively), a bulk Sn foil taken at 20 K. The grey dashed line indicates the full width at half maximum of the experimental resolution function.

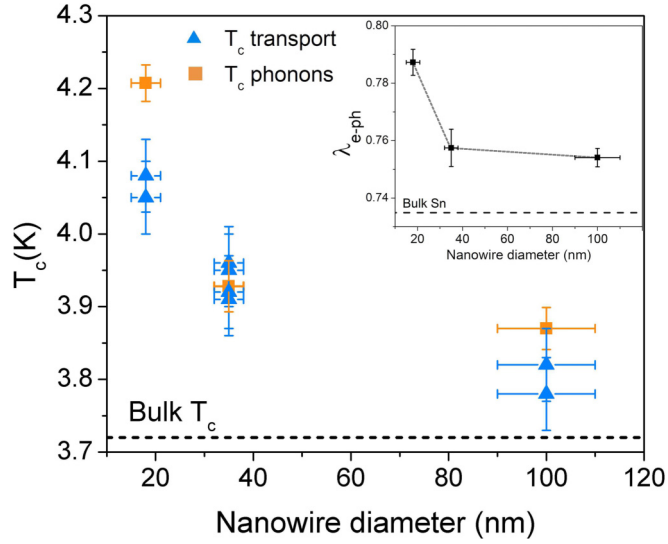

FIG. 7. Comparison between T_c derived from transport and phonon measurements. The inset shows the evolution of the electron-phonon coupling parameter as a function of the nanowire diameter.

16.5 meV is noticeably lower for the three diameters studied. Furthermore, the peak structure is completely broadened in the 100 nm and 18 nm $F(E)$. In the medium energy region, between 7–14 meV, an increase of the phonon modes occurs, especially in the 18 nm sample. Moreover, the intensity of the low-energy modes, between 0–3 meV, is also enhanced. This feature is better appreciated in Fig. 6, which shows how this enhancement is more pronounced as the diameter of the wires decreases. On the other hand, the intensity of the peak at 5 meV is considerably reduced. Finally, a number of modes extending beyond the cutoff energy 18.5 meV are visible. These differences observed between the Sn foil $F(E)$ and the Sn nanowires $F(E)$ are caused by the structural and morphological differences between the different samples.

V. DISCUSSION

Using the measured $F(E)$'s it is possible to calculate how the changes in $F(E)$ with respect to bulk affect T_c. The superconducting critical temperature can be calculated using the Allen-Dynes equation [43], which is a correction of the McMillan expression for the T_c of conventional superconductors.

$$T_c = \frac{f_1 f_2 \omega_{\log}}{1.2} e^{-\frac{1.04(1+\lambda_{\text{e-ph}})}{\lambda_{\text{e-ph}} - \mu^* - 0.62\lambda_{\text{e-ph}}\mu^*}}, \tag{2}$$

where the electron-phonon coupling constant is calculated as

$$\lambda_{\text{e-ph}} = 2\int \frac{\alpha^2(E)F(E)}{E} dE \tag{3}$$

the logarithmic frequency average is

$$\omega_{\log} = e^{\frac{2}{\lambda_{\text{e-ph}}}\int \frac{\alpha^2(E)F(E)}{E}\ln(E)dE} \tag{4}$$

and the prefactors, that depend on the characteristic phonon frequency, are

$$f_1 = \left[1 + \left(\frac{\lambda_{\text{e-ph}}}{2.46(1+3.8\mu^*)}\right)\right]^{1/3},$$

$$f_2 = 1 + \frac{\lambda_{\text{e-ph}}^2\left(\frac{\langle\omega^2\rangle^{1/2}}{\omega_{\log}} - 1\right)}{\lambda_{\text{e-ph}}^2 + \left[1.82\left(1 + 6.3\mu^*\frac{\langle\omega^2\rangle^{1/2}}{\omega_{\log}}\right)\right]}, \tag{5}$$

$$\langle\omega^2\rangle = \frac{2}{\lambda_{\text{e-ph}}}\int \alpha^2(E)F(E)E dE.$$

The electron-phonon coupling strength function $\alpha^2(E)$, shown in Ref. [23], has been calculated from the ratio between the Eliashberg function $\alpha^2(E)F(E)$ determined from electron tunneling measurements [20] and $F(E)$ of a Sn foil that we previously measured [42]. This method has also been successfully applied in order to estimate the form of $\alpha^2(E)$ in Nb_3Sn thin films [19]. The value of μ^* is fixed to 0.107 and is chosen to yield the bulk T_c value 3.7 K when the bulk Sn $F(E)$ is used in the calculation. The chosen value of μ^* agrees with the values found in literature [44]. The same μ^* and $\alpha^2(E)$ were subsequently used to calculate T_c for the nanowires. Values of 4.20 ± 0.03, 3.93 ± 0.04, and 3.87 ± 0.03 K are found for the 18 nm, 35 nm, and 100 nm nanowires, respectively. Figure 7 shows a comparison between T_c obtained from the transport measurements, T_c obtained using the experimentally derived $F(E)$, and the bulk Sn T_c. The values of T_c for the 100 nm and 35 nm samples obtained in the transport measurements are in agreement with the values calculated using the phonon density of states. In the case of the 18 nm nanowires, a deviation occurs.

The value of the electron-phonon coupling parameter $\lambda_{\text{e-ph}}$ is displayed in the inset of Fig. 7. Similarly to the trend observed in T_c, $\lambda_{\text{e-ph}}$ increases as the diameter is reduced. More specifically, an increase between 2.5% and 4.7% with respect to bulk Sn is obtained. This enhancement originates

from the phonon softening effects. Calculations of the characteristic phonon frequency $\langle\omega^2\rangle^{1/2}$, shown in Fig. 5, indicate that there is a shift of the phonon frequencies towards the low-energy region. Low-energy phonons have a bigger impact on $\lambda_{\text{e-ph}}$ than high energy phonons due to the fact that the spectrum $\alpha^2(E)F(E)$ is weighted by a factor $1/E$. Phonon softening specially affects nanoscale materials because the ratio of surface to volume atoms is higher than in bulk. These surface atoms are characterized for having lower vibrational frequencies than the bulk ones, known as surface modes [45,46], which shifts the phonon spectrum to the low-energy region. While T_c and $\lambda_{\text{e-ph}}$ increase monotonically as the diameter is reduced, it is not the case for $\langle\omega^2\rangle^{1/2}$. The discrepancy arises from the shape of $F(E)$ at high energies. As can be seen in Fig. 5, the $F(E)$ shape of the 35 nm sample around 15 meV resembles much more bulk Sn than in the case of the 100 nm nanowires. The contribution of these phonon modes to $\langle\omega^2\rangle^{1/2}$ is more relevant than the low-energy ones since, as Eq. (5) shows, the spectrum $\alpha^2(E)F(E)$ is weighted by a factor E. Nevertheless, T_c depends on more quantities apart from $\langle\omega^2\rangle^{1/2}$. A small deviation in one of the parameters can be compensated by the others, resulting in a T_c enhancement.

Despite the good correspondence between the T_c trend obtained from transport measurements and the one calculated using the phonon spectra, the correspondence between $T_{c,\text{transport}}$ and $T_{c,\text{phonons}}$ of the 18 nm sample is less good. Quantum size effects are no longer negligible in Sn nanosystems once the sample size reduces below $d \leqslant \sqrt{\frac{\hbar^2\pi^2}{2m_e\Delta_{bulk}}} \backsim 26$ nm [47]. In the case of Sn nanowires, these effects are significant for diameters below 20 nm [48]. Our calculations using $F(E)$ only account for the impact of phonon confinement on T_c, not QSE. Hence, QSE could slightly offset the electron-phonon coupling enhancement caused by phonon softening [13]. Ultimately, T_c will be enhanced but it will be limited by the interplay between phonon softening and QSE.

The interaction between the nanowires and the Al_2O_3 matrix is expected to influence the T_c enhancement. Al_2O_3 is harder than Sn since the vibrational spectrum of Al_2O_3 spans up to 120 meV [49], therefore, the Al_2O_3 matrix is expected to reduce the number of surface phonon modes as compared to the case of free standing nanowires, limiting the effects of phonon softening without suppressing them completely. This is analogous to the case of nanoparticles capped with a hard layer, the number of surface modes that shifts towards lower energies is smaller than in the case of free particles [50], since the energy of the nanoparticle surface modes is increased by the interaction with the capping layer. Moreover, Bessas *et al.* measured the phonon density of states of Bi_2Te_3 nanowires with a diameter of 56 nm embedded in Al_2O_3 [51]. No significant differences were found when comparing the phonon density of states of the nanowires to the one of bulk Bi_2Te_3. Their analysis concluded that the Debye level ($\lim_{E\to 0} F(E)/E^2$) of the nanowires was higher than the Debye level of bulk Bi_2Te_3, which caused a decrease of the nanowire sound velocity of 6.5%. They attributed this reduction to confinement due to nanostructuring. In addition, they estimated that only phonons with an energy of 0.12 meV will be affected by interactions with the Al_2O_3 matrix. This leads to the conclusion that the Al_2O_3 matrix does not strongly interact with the Bi_2Te_3.

Note that the phonon density of states of Sn and Te are quite similar, both of them show a phonon energy cutoff around 18 meV and the Debye behavior extends only up to 4 meV. Moreover, similarly to the case of Bi_2Te_3 nanowires, the Debye level of Sn nanowires is higher than the one of bulk Sn. Finally, the number of Al_2O_3 phonon modes available to interact with the Sn phonon modes is small, since the Sn phonon cutoff occurs at 18 meV, while the majority of the phonon modes in Al_2O_3 occurs above 25 meV. These features suggest that there is not a strong interaction between the Al_2O_3 matrix and Sn nanowires and that the differences between the Sn nanowires $F(E)$ and the bulk Sn $F(E)$ are a consequence of the nanostructuring.

Phonon softening affects any superconducting nanostructure, regardless of its coupling strength. As mentioned before, T_c of weak-coupling superconductors increases upon size reduction while no impact or even a reduction of T_c is observed in strong coupling materials. Note that, according to theoretical calculations, strong-coupling superconducting nanograins exhibit a larger broadening of single electron levels and a heavier electron mass than weak-coupling superconductors [52]. QSE are inversely proportional to the electron mass, thus making them more relevant in strong-coupling superconductors. Then, QSE could offset or even overcome the effect of phonon softening in strong-coupling materials, resulting in an unaffected value of T_c.

In summary, for the first time the phonon density of states of Sn nanowires with diameters of 18, 35, and 100 nm has been experimentally determined and used to calculate their T_c. The correspondence between the critical temperature measured by transport measurements and the one calculated from the measured $F(E)$ suggests that phonon softening plays a significant role in the T_c enhancement, although other effects, in particular electron confinement, might also affect the T_c of the smallest nanowires investigated. In addition, our results provide a direct correlation between phonon confinement effects, the modification of the electron-phonon coupling strength $\lambda_{\text{e-ph}}$ and the T_c enhancement of a weak-coupling superconductor. Further research on the modifications of $F(E)$ in both, weak and strong-coupling nanoscale superconductors, as well as the shape of $\alpha^2(E)$ will help to understand the specific roles of phonon and electronic confinement. Our work enables the quantification of phonon softening effects, assessing its impact in the modification of the electron-phonon coupling strength at the nanoscale.

ACKNOWLEDGMENTS

We would like to thanks Jeroen Scheerder and Wout Keijers for their help and assistance during the low-temperature measurements. This work was supported by the Research Foundation Flanders (FWO), the Concerted Research Action (GOA/14/007), the Fédération Wallonie-Bruxelles (ARC 13/18-052, Supracryst) and the Fonds de la Recherche Scientifique – FNRS under Grant No. T.0006.16. The authors acknowledge Hercules Stichting (Project Nos. AKUL/13/19 and AKUL/13/25). D.P.L. thanks the FWO for financial support. This research used resources of the Advanced Photon

Source, a US Department of Energy (DOE) Office of Science User Facility operated for the DOE Office of Science by Argonne National Laboratory under Contract No. DE-AC02-06CH11357.

[1] A. D. Wright, C. Verdi, R. L. Milot, G. E. Eperon, M. A. Pérez-Osorio, H. J. Snaith, F. Giustino, M. B. Johnston, and L. M. Herz, Nat. Commun. **7**, 11755 (2016).

[2] T. Wang, Z. Gui, A. Janotti, C. Ni, and P. Karandikar, Phys. Rev. Mater. **1**, 034601 (2017).

[3] J. Bardeen, L. N. Cooper, and J. R. Schrieffer, Phys. Rev. **108**, 1175 (1957).

[4] S. Bose and P. Ayyub, Rep. Prog. Phys. **77**, 116503 (2014).

[5] S. Dubois, A. Michel, J. P. Eymery, J. L. Duvail, and L. Piraux, J. Mater. Res. **14**, 665 (1999).

[6] M. He, C. H. Wong, P. L. Tse, Y. Zheng, H. Zhang, F. L. Y. Lam, P. Sheng, X. Hu, and R. Lortz, ACS Nano **7**, 4187 (2013).

[7] S. Bose, A. M. García-García, M. M. Ugeda, J. D. Urbina, C. H. Michaelis, I. Brihuega, and K. Kern, Nat. Mater. **9**, 550 (2010).

[8] P. B. Allen, in *Handbook of Superconductivity*, edited by C. P. Poole, Jr. (Academic Press, New York, 1999), Ch. 9, Sec. G, pp. 478–483.

[9] F. Altomare, A. M. Chang, M. R. Melloch, Y. Hong, and C. W. Tu, Phys. Rev. Lett. **97**, 017001 (2006).

[10] M. Tian, J. Wang, J. S. Kurtz, Y. Liu, M. H. W. Chan, T. S. Mayer, and T. E. Mallouk, Phys. Rev. B **71**, 104521 (2005).

[11] F. Y. Wu, C. C. Yang, C. M. Wu, C. W. Wang, and W. H. Lia, J. Appl. Phys **101**, 09G111 (2007).

[12] B. Abeles, R. W. Cohen, and G. W. Cullen, Phys. Rev. Lett. **17**, 632 (1966).

[13] S. Bose, C. Galande, S. P. Chockalingam, R. Banerjee, P. Raychaudhuri, and P. Ayyub, J. Phys.: Condens. Matter **21**, 205702 (2009).

[14] G. C. Tettamanzi, C. I. Pakes, A. Potenza, S. Rubanov, C. H. Marrows, and S. Prawer, Nanotechnology **20**, 465302 (2009).

[15] P. P. Parshin, M. G. Zemlyanov, G. Kh. Panova, A. A. Shikov, A. A. Naberezhnov, Yu. A. Kumzerov, I. V. Golosovsky, and A. S. Ivanov, J. Exp. Theor. Phys. **111**, 996 (2010).

[16] M. D. Croitoru, A. A. Shanenko, and F. M. Peeters, Phys. Rev. B **76**, 024511 (2007).

[17] M. Strongin, O. F. Kammerer, J. E. Crow, R. D. Parks, D. H. Douglass, Jr., and M. A. Jensen, Phys. Rev. Lett. **21**, 1320 (1968).

[18] P. P. Parshin, M. G. Zemlyanov, G. Kh. Panova, A. A. Shikov, Yu. A. Kumzerov, A. A. Naberezhnov, I. Sergueev, W. Crichton, A. I. Chumakov, and R. Rüffer, J. Exp. Theor. Phys. **114**, 440 (2012).

[19] S. Couet, H. Peelaers, M. Trekels, K. Houben, C. Petermann, M. Y. Hu, J. Y. Zhao, W. Bi, E. E. Alp, E. Menéndez, B. Partoens, F. M. Peeters, M. J. Van Bael, A. Vantomme, and K. Temst, Phys. Rev. B **88**, 159903(E) (2013).

[20] J. M. Rowell, W. L. McMillan, and W. L. Feldmann, Phys. Rev. B **3**, 4065 (1971).

[21] L. Zaraska, E. Kurowska, G. D. Sulka, and M. Jaskua, Appl. Surf. Sci. **258**, 9718 (2012).

[22] M. Tian, N. Kumar, S. Xu, J. Wang, J. S. Kurtz, and M. H. W. Chan, Phys. Rev. Lett. **95**, 076802 (2005).

[23] See Supplemental Material at http://link.aps.org/supplemental/10.1103/PhysRevB.99.064512 for details on the transport measurements and the phonon density of states when the x-ray beam is parallel and perpendicular to the nanowires axis.

[24] L. Lutterotti and P. Scardi, J. Appl. Crys. **23**, 246 (1990).

[25] MAUD (Materials Analysis Using Diffraction), http://maud.radiographema.com/.

[26] B. D. Cullity, *Elements of X-ray Diffraction* (Addison-Wesley, Reading, MA, 1956), p. 262.

[27] L. Jankovič, D. Gournis, P. N. Trikalitis, I. Arfaoui, T. Cren, P. Rudolf, M. Sage, T. T. M. Palstra, Bart Kooi, J. De Hosson, Mi. A. Karakassides, K. Dimos, A. Moukarika, and T. Bakas, Nano Lett. **6**, 1131 (2006).

[28] Y. Zhang, C. Ho Wong, J. Shen, S. T. Sze, B. Zhang, H. Zhang, Y. Dong, H. Xu, Z. Yan, Y. Li, X. Hu, and R. Lortz, Sci. Rep. **6**, 32963 (2016).

[29] C. Kittel, *Introduction to Solid State Physics* (Wiley, New York, 1986).

[30] M. Tian, J. Wang, J. Snyder, J. Kurtz, Y. Liu, P. Schiffer, T. E. Mallouk, and M. H. W. Chan, Appl. Phys. Lett. **83**, 1620 (2003).

[31] V. V. Moshchalkov and J. Fritzsche, in *Nanostructured Superconductors*, 1st ed., edited by V. V. Moshchalkov (World Scientific, Singapore, 2011), Chap. 2.

[32] V. V. Moshchalkov, L. Gielen, C. Strunk, R. Jonckheere, X. Qiu, C. Van Haesendonck, and Y. Bruynseraede, Nature (London) **373**, 319 (1995).

[33] M. Tinkham, in *Introduction to Superconductivity*, 2nd ed., edited by M. Tinkham (McGraw-Hill, New York, 1975).

[34] S. Bose, P. Raychaudhuri, R. Banerjee, and P. Ayyub, Phys. Rev. B **74**, 224502 (2006).

[35] L. Fàbrega, A. Camón, I. Fernández-Martínez, J. Sesé, M. Parra-Borderías, O. Gil, R. González-Arrabal, J. L. Costa-Krämer, and F. Briones, Supercond. Sci. Technol. **24**, 075014 (2011).

[36] A. Chumakov and W. Sturhahn, Hyperfine Interact. **123**, 781 (1999).

[37] R. Röhlsberger, J. Phys.: Condens. Matter **13**, 7659 (2001).

[38] B. M. Leu, M. Sturza, M. Y. Hu, D. Gosztola, V. Baran, T. F. Fässler, and E. E. Alp, Phys. Rev. B **90**, 104304 (2014).

[39] W. Sturhahn, J. Phys.: Condens. Matter **16**, S497 (2004).

[40] W. Sturhahn, Hyperfine Interact. **125**, 149 (2000).

[41] V. G. Kohn, A. I. Chumakov, and R. Rüffer, Phys. Rev. B **58**, 8437 (1998).

[42] K. Houben, Ph.D. thesis, KU Leuven, 2015.

[43] P. B. Allen and R. C. Dynes, Phys. Rev. B **12**, 905 (1975).

[44] R. C. Dynes, Solid State Commun. **10**, 615 (1972).

[45] S. Stankov, R. Röhlsberger, T. Ślęzak, M. Sladecek, B. Sepiol, G. Vogl, A. I. Chumakov, R. Rüffer, N. Spiridis, J. Łażewski, K. Parliński, and J. Korecki, Phys. Rev. Lett. **99**, 185501 (2007).

[46] K. Houben, S. Couet, M. Trekels, E. Menéndez, T. Peissker, J. W. Seo, M. Y. Hu, J. Y. Zhao, E. E. Alp, S. Roelants, B. Partoens, M. V. Miloševic, F. M. Peeters, D. Bessas, S. A. Brown, A. Vantomme, K. Temst, and M. J. Van Bael, Phys. Rev. B **95**, 155413 (2017).

[47] F. M. Peeters, A. A. Shanenko, and M. D. Croitoru, in *Handbook of Nanophysics: Principles and Methods*, 1st ed., edited by K. D. Sattler (CRC Press, Boca Raton, 2010), Chap. 9, pp. 9.1–9.32.
[48] A. A. Shanenko, M. D. Croitoru, M. Zgirski, F. M. Peeters, and K. Arutyunov, Phys. Rev. B **74**, 052502 (2006).
[49] S. Davis and G. Gutiérrez, J. Phys.: Condens. Matter **23**, 495401 (2011).
[50] A. Tamura, Z. Phys. D **26**, 240 (1993).
[51] D. Bessas, W. Töllner, Z. Aabdin, N. Peranio, I. Sergueev, H. Wille, O. Eibl, K. Nielsch, and R. P. Hermann, Nanoscale **5**, 10629 (2013).
[52] M. D. Croitoru, A. A. Shanenko, A. Vagov, M. V. Milošević, V. M. Axt, and F. M. Peeters, Sci. Rep. **5**, 16515 (2015).